RESEARCH ARTICLE

Small catchments: remote sensing approach for environmental research in the High Arctic

Aleksandra Wołoszyn,[1,2] Iwo Wieczorek[2,3] & Marek Kasprzak[2]

[1]Department of Geoinformatics and Applied Computer Science, Faculty of Geology, Geophysics, and Environmental Protection, AGH University of Krakow, Kraków, Poland; [2]Alfred Jahn Cold Regions Research Centre, Faculty of Earth Sciences and Environmental Management, University of Wrocław, Wrocław, Poland; [3]Department of Physical Geography and Geoecology, Charles University, Prague, Czech Republic

Abstract

This study examines the morphometric characteristics and environmental changes in 143 small catchments within Wedel Jarlsberg Land, southern Svalbard, focusing on the influence of topography on glacier retreat, lake evolution, and vegetation dynamics. The catchments analysed varied in size, with 65% smaller than 4 km². Elevation ranged from 1.9 to 1200 m a.s.l., and the catchments exhibited significant topographic variability, including steep slopes and varying exposures. Glaciers in the study area have undergone a 30% reduction in area from 1936 (228.34 km²) to 2020 (158.26 km²). This retreat has led to the expansion of glacial lakes, particularly within moraines, with a general trend towards increasing numbers and sizes of lakes over time. Vegetation changes were assessed using normalized difference vegetation index data from 1979 to 2020, revealing few increasing trends. Topographical features, including mean elevation, slope and catchment size, were analysed to understand their impact on glacial retreat and vegetation growth. The study found that mean slope and aspect had the strongest influence on vegetation dynamics, and that mean elevation and slope values have an impact on glacial retreat in the High Arctic.

Keywords

NDVI; NDSI; Svalbard; glacial retreat; vegetation; catchment morphometry

Correspondence

Aleksandra Wołoszyn, Department of Geoinformatics and Applied Computer Science, Faculty of Geology, Geophysics, and Environmental Protection, AGH University of Krakow, Al. Mickiewicza 30, Pawilon A-0, 30-059 Kraków, Poland. E-mail: awoloszyn@agh.edu.pl

Abbreviations

NDSI: normalized difference snow index
NDVI: normalized difference vegetation index
SC: small water catchment
WJL: Wedel Jarlsberg Land

To access the supplementary material, please visit the article landing page

Introduction

The Arctic is rapidly warming (Speetjens et al. 2022) and has warmed nearly four times faster than the globe in recent decades (Rantanen et al. 2022). The Eurasian part of the Arctic has warmed at an even higher rate: five to seven times faster than the global average (Isaksen et al. 2022; Rantanen et al. 2022; Tobo et al. 2024). The phenomenon of faster reaction to global warming at higher latitudes is known as Arctic (or Polar) Amplification (Smith et al. 2019; Rantanen et al. 2022) and is manifested in diminishing sea-ice cover, glacial terminus retreat (sometimes resulting in shifts from tidewater to land-terminating glaciers), more streams and lakes associated with retreating glaciers, intensification of mass movement, advances of vegetation and permafrost thawing (Constable et al. 2022). In the High Arctic, Svalbard is known as a hotspot where the environmental effects of higher global temperature are readily observed (McKay et al. 2022; Stachowska et al. 2024). Climate change is apparent in both higher temperatures and humidity, noticeable as an increase in precipitation in the archipelago (Førland & Hanssen-Bauer 2001). This is mainly reflected in retreating glaciers, which expose new land areas that are well suited to vegetation succession studies (Bayle et al. 2021; McCerery et al. 2025). As the warming Arctic has both local and global influences, understanding its impact is crucial as the landscape-scale changes are superimposed on large-scale Arctic responses (Box et al. 2019; Vincent 2020; Yamanouchi & Takata 2020; Speetjens et al. 2022; Frost et al. 2025). Moreover, the dynamics of change within small catchments affect hydrological regimes (Stachnik et al. 2025).

All the features mentioned above lead to visible changes in the Arctic landscape. The first photogrammetric campaigns in the Arctic took place in the 1930s and have been used for glaciological reconstruction (Geyman et al. 2022; Dømgaard et al. 2024). Since the late 1970s, multispectral satellite images of Svalbard's environment have been captured. This has resulted in a long-term multispectral image series of the archipelago. Landsat data have been freely

Citation: *Polar Research* 2026, *45*, 12280, http://dx.doi.org/10.33265/polar.v45.12280

available since 2008, and Sentinel data sets since 2014. These long-term data sets are invaluable for understanding change in remote regions (Trenberth et al. 2013; Roy et al. 2014; Roy et al. 2016; Wulder et al. 2022).

We aimed to better understand how climate change impacts small (here defined as <20 km^2) Arctic watersheds, as they are highly responsive to climate change, and the pronounced changes in hydrography and vegetation that are documented in this study could be considered as potential forerunners for other parts of the Arctic as well as alpine regions (Vonk et al. 2023). We investigated SCs with a 40-year (1979–2020) perspective, focusing on vegetation (NDVI changes), glaciers (areal changes), and lakes (formation and dynamics). Data extending back to 1936/38 were also included. Additionally, using remote sensing data sets, we investigated if the topography, that is, basic morphometric features, of each SC influences the rate of glacier retreat and the pace of vegetation growth. Our study focused on WJL, Spitsbergen (Figs. 1, 2), and provides the first regional-scale analysis of this area.

Methods

Study area and geographical setting

WJL is in south-western Svalbard, on the island of Spitsbergen (Fig. 1). Covering an area of ca. 2150 km^2, it stretches between Bellsund and Van Keulenfjorden in the north and Hornsund in the south, bordering on Torell Land in the east and the Greenland Sea in the west. Together with Torell Land and Sørkapp Land, WJL is part of Sør Spitsbergen National Park. The main sedimentary rock types are sandstone, siltstone, shales, and bituminous shales in the north-east, tillite rocks at the Bellsund inlet, metamorphic rocks in the west, and phyllites, metapeltic shists, metavolcanic amphibolites, and quartzites in the south-west (Dallmann 2015; Supplementary Fig. S1). Soils comprise both Cambisols and Cryosols (Speetjens et al. 2022). The sparse vegetation cover consists mainly of mosses, shrubs, and lichens (Supplementary Fig. S2). The alpine landscape is dominated by numerous moraines and talus cones, small glaciers and spiky peaks (Dallmann 2015; Supplementary Fig. S3), the highest of which is 1230 m a.s.l. The inner part of WJL is covered by ice fields, with few outgoing tidewater glaciers (Fig. 1). During winter, the area is covered in snow, and lakes are frozen. During spring and summer, thawing permafrost and melting snow and glaciers feed numerous streams and ponds. Lakes are mostly moraine-dammed (moraine-thaw and frontal moraine-dammed, otherwise known as end-moraine lakes), which have increased in number by 23% between 1936 (Geyman et al. 2022) and 2020 (Wieczorek et al. 2023). The warm West Spitsbergen Current results in a milder climate (D'Andrea et al. 2012; Dallmann 2015) and more precipitation (Wawrzyniak & Osuch 2020) in south-western Spitsbergen than in other places at similar latitudes. A 40-year-long (1979–2018) meteorological data series from the Polish Polar Station in Hornsund showed an increase in temperature of 1.14°C each decade, which is six times the global average (Wawrzyniak & Osuch 2020). Climatic changes have resulted in a transition in the area from glaciated to partly glaciated to non-glaciated, as observed for Svalbard overall (Lønne & Lysså 2005).

Catchment delimitation. There are no universal and precise size limits for small, medium, or large catchments; these depend on the size of the area studied. In a pan-Arctic database, small watersheds were defined as smaller than 1000 km^2 (Speetjens et al. 2022). We considered delineating SCs on the basis of the following digital terrain models available for WJL: one from 1936 has a resolution of 5-m (Geyman et al. 2022), one from the 1990s has 20-m resolution (NPI 2014b), one from 2011 has 5-m resolution (NPI 2014b) and one—the ArcticDEM, version 4.1 (PGC, Saint Paul, MN, USA)—from 2023 has 2-m resolution (Porter et al. 2023).

Results from the digital terrain models varied due to differences in resolution and changes in geomorphology over time. We chose the ArcticDEM because it yielded the most satisfactory results. The ArcticDEM raster overestimates elevation in WJL. Based on different stable points, that is, large rocks and mountain peaks, which we compared between the ArcticDEM and topographic maps, we estimated 30 m as the mean value of vertical distortion. We followed the procedure recommended for Arc Hydro Tools for the final SC delineation (ESRI 2011; Baye 2020; Fig. 2). A crucial point was the stream definition step (set to 1 km^2), which defines where a stream should start without any feedback from the function (ESRI 2011; Baye 2020) and directly influences the catchment area. The SCs—including those that were ice-free, partially glaciated, and entirely glaciated—that were delineated are presented in Fig. 1. Catchments on the surface of ice fields and in valleys were then removed from consideration, and sub-catchments were merged, leaving only alpine catchments. We refer to most of these SCs by the Hydro Identifier number assigned to each during SC delineation. However, if there was a valley name or a named glacier within an SC, we called it by that name. The morphometric features of SCs were used later to investigate their impact on vegetation succession and glacial recession. For each SC, the basic morphometric parameters (Table 1) were calculated using Arc Toolbox in ArcMap 10.8 (Esri, Redlands, CA, USA). Seventeen of the 143 SCs that we analysed have been previously studied.

Citation: *Polar Research* 2026, *45*, 12280, http://dx.doi.org/10.33265/polar.v45.12280

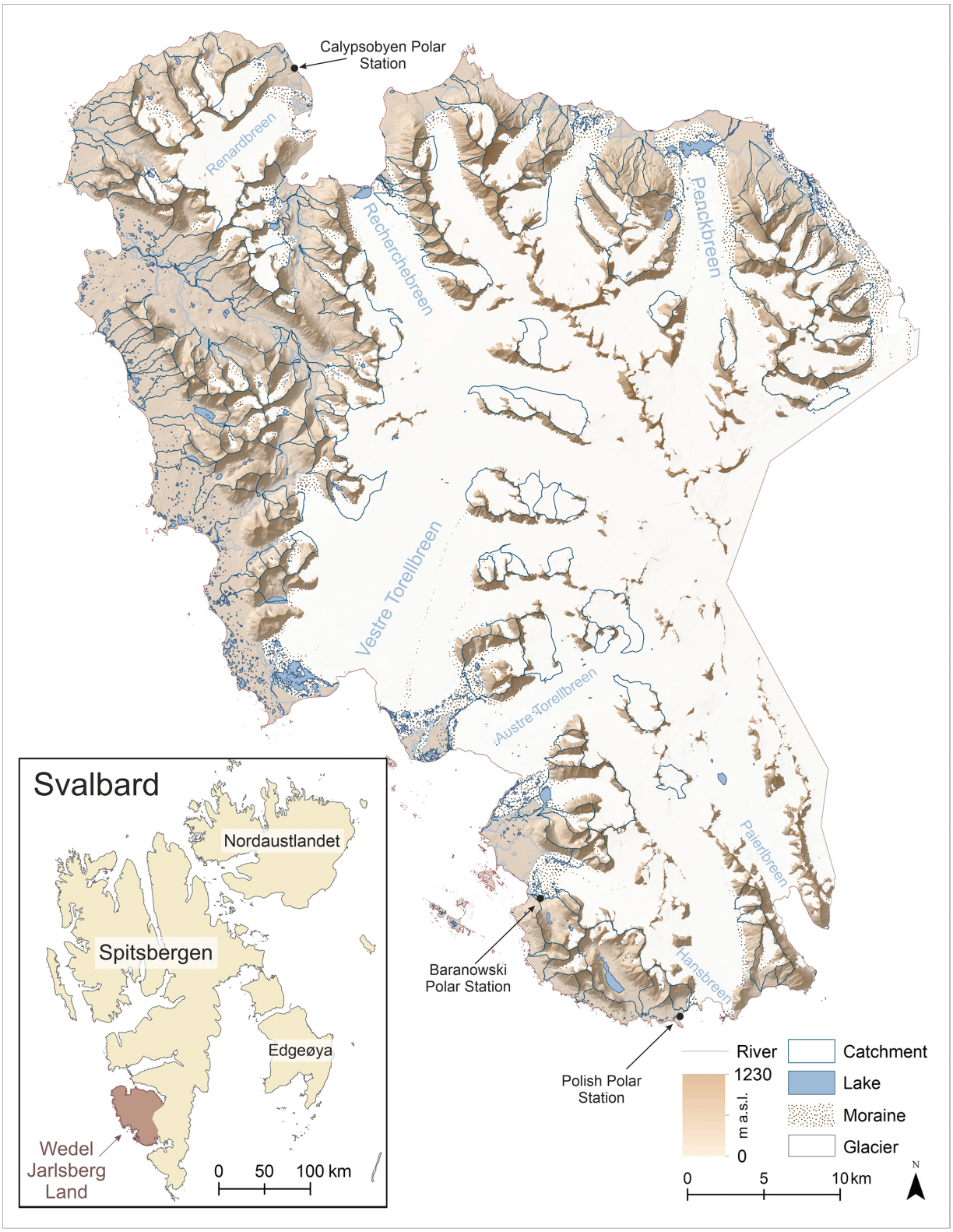

Fig. 1 Location and land characteristics of the WJL and designated SCs within the area. The coverage of rivers, glaciers, lakes, moraines, and the area of Svalbard was downloaded from the Norwegian Polar Institute (NPI 2014a), and the digital elevation model is based on ArcticDEM version 4.1 (Porter et al. 2023).

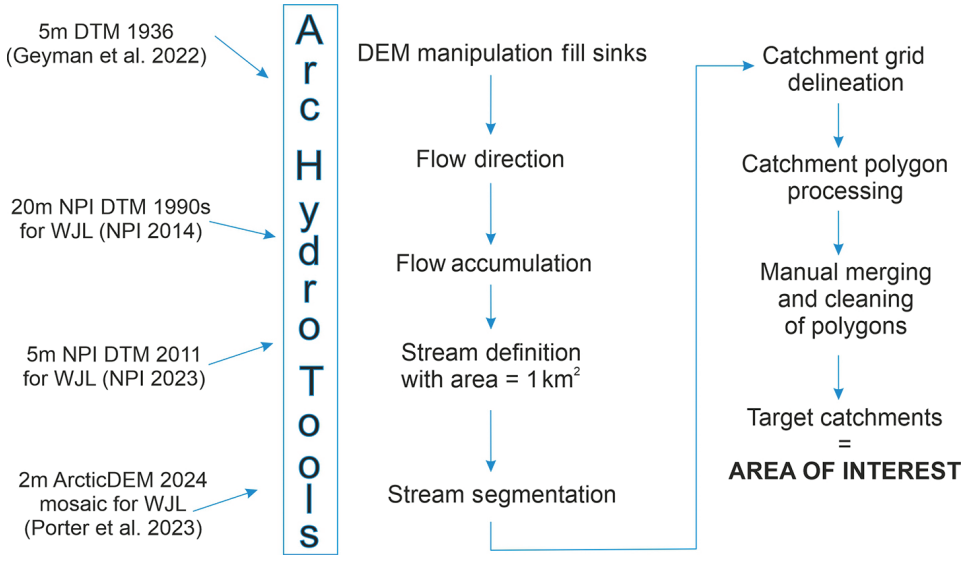

Fig. 2 Methodology of catchment delineation.

Table 1 Investigated morphometric parameters.

Morphometric parameter	Tool/method	Equation	Source
Area (A)	Calculate geometry		
Perimeter (P)	Calculate geometry		
Basin length (L)	ArcHydroTools, longest flow path		
Slope (°)	Spatial Analyst tool, Slope		
Aspect	Spatial Analyst tool, Aspect		
Elevation (min., mean, max.)	Focal statistics		
Relief		$H_{max} - H_{min}$	
Relief ratio		$\frac{H}{L}$	Schumm 1956; Różycka & Migoń 2021; Alphonse et al. 2023
Circulatory ratio		$\frac{4\pi A}{P^2}$	Różycka & Migoń 2021; Alphonse et al. 2023
Elongation ratio		$\frac{2A/\sqrt{\pi}}{L}$	Schumm 1956; Różycka & Migoń 2021; Alphonse et al. 2023
Form factor		$\frac{A}{L^2}$	Horton 1932; Różycka & Migoń 2021; Alphonse et al. 2023

Remote sensing methods. For remote sensing analysis, we chose normalized difference indices as they help minimize the influence of sensor calibration, sun-sensor geometry and topography (Kääb 2005; Frost et al. 2025). To observe vegetation changes within the SCs, we used the NDVI (Tucker 1979). The analysis used atmospheric-corrected Landsat satellite scenes (61 scenes) from Landsat Collection 2 (MSS 2, 5; TM 4, 5; ETM+ 7; OLI 8 sensors) and Sentinel-2 (three hand-made mosaics at 15-m resolution for the years 2017, 2018 and 2020). WJL is covered by the following Landsat satellite flight paths and rows: 027240, 028239, 029239, 208005, 209005, 210005, 211005, 212005, 213004, 215004, 216004, 228005, 229004, 229005, 230004, and 234004. Due to the prevalence of cloud cover, the mosaic for the Sentinel satellite data from 2018 was compiled using images captured on 30 July and 5 August. We used only images from the summer months of July and August. All available Landsat images were browsed without a cloud filter, as we were focusing on very small areas, and

Citation: *Polar Research* 2026, *45*, 12280, http://dx.doi.org/10.33265/polar.v45.12280

generalizing percentages of cloud cover could have caused us to miss valuable data. After revising the collected data, we obtained images from 56 days in the period 1979–2020. All processing was calculated with Python 2 for all available images in ArcMap 10.8. We used the following raster calculator formula:

NDVI = float (nir_band – red_band) / float (nir_band + red_band)

The near-infrared and red bands have previously been defined for each satellite type (USGS 2021; Wołoszyn 2024; Sentinel Hub no date a). Results were then clipped with Image Analysis in ArcMap to all delineated SCs. Only SCs with no cloud or snow cover in July were included in the analysis; the rest were filtered out manually. Only data where 100% of a single SC was visible were used. The number of satellite images available for a given SC depended on the prevalence of cloud cover and the number of pathways traversed by the satellite. Our objective was to obtain as much data as possible to best capture changes in the study area. The number of analysed SCs captured on specific dates is presented in Supplementary Fig. S4.

For each SC, a histogram was constructed to compare data across different time spans and to identify any errors or anomalies in the data. This approach led to a long time series of data for each individual SC. For more recent years, we added Sentinel data and mosaicked single images so that most WJL SCs were visible. We then obtained the maximum catchment NDVI values so that a temporal analysis of vegetation cover in WJL's SCs could be made.

The Mann–Kendall tests were performed to identify any trends, as the data contains gaps, and this test effectively handles them. A significance level of 0.05 was assumed.

For glacier delineation, we used the NDSI (Keshri et al. 2009; Hagolle et al. 2017; Florath et al. 2022):

NDSI = float (green_band – swir_band) / float (green_band + swir_band)

The NDSI was applied as a tool for determining the glacial area and, to indicate their response to climate change (Nuth et al. 2013). Given the potential for misinterpreting snow-covered slopes, only data from August—just once, at—the end of July—were used. This minimized—but did not completely exclude—snow-covered ground. To delineate the extent of the glaciers by creating polygons, a threshold of 0.0 was set for the index values, filtering out pixels that were neither snow nor glacier. Subsequently, following the conversion of the float raster to an integer and then to a polygon, the automatically-determined extents of the glaciers were manually corrected on the basis of the reflectance band for each image. In total, 22 satellite scenes were used, along with data from 1936 (Geyman et al. 2022) and the 1990s (NPI 2014a). We then sequentially counted changes in how much (percentage) of an SC was occupied by glaciers. Only the 97 SCs that were glaciated in 1936 (Geyman et al. 2022) were taken into account.

Lakes were manually vectorized based on the 1936/38 orthophotomap, the 1990 data set (Wieczorek et al. 2023), the Norwegian Polar Institute orthophotomap from 2011 (NPI 2014b) and enhanced Planet images from 2016, 2017, 2018, 2019, and 2020. The resolution of the Landsat and Sentinel images is too coarse for such small areas; therefore, the data set we used for lakes differs from the one used for glaciers and vegetation.

Methods of comparing morphometric and remote sensing results. To examine spatial relationships, we used scatterplots based on the morphometric and remote sensing results we had obtained. To assess the influence of morphometry on the remote sensing results, we used the percentage decrease in glacier area and the difference in maximum catchment NDVI between 1979 and 2020. For glaciers, we used only data in which some change—positive or negative—occurred. For vegetation, all SCs were considered. First, scatterplots were generated for each parameter in Statistica 13 software (StatSoft, Palo Alto, CA, USA) to visualize the relationship between the pairs, that is, glacial area difference and vegetation change as dependent variables (y-axis) and morphometric features as explanatory variables (x-axis). For the aspect, we used the majority value within SCs. The results of the comparative analyses for this aspect were visualized using box and whisker plots. Then, the Multilayer Perception machine learning tool (MathWorks 2025, Natick, MA, USA) was applied to analyse existing relationships.

Results

Catchment morphometry

A total of 143 SCs were delineated and their morphometrical parameters recorded (Supplementary Table S1; Supplementary Fig. S5). The majority of the analysed SCs were smaller than 10 km², and nearly one-third were no larger than 2 km². (Supplementary Fig. S5a). Only eight SCs were larger than 10 km²: Dyrstaddalen, Scottdalen, Hessdalen, Märjelendalen, Suessdalen, Langryggdalen, Raudfjelldalen, and Nanndalen. Most SCs were between 2 and 9 km in length (Supplementary Fig. S5b). This parameter was used to calculate other morphometric features (Table 1). The mean width (Supplementary Fig. S5d) ranged from 0.3 to 2 km; most SCs were between 0.4 and 0.8 km wide.

The SCs varied in elevation. The lowest parts of the SCs ranged from 1.9 to 570.4 m a.s.l., while their highest parts ranged from 343 to 1200 m a.s.l. Their mean altitudes spanned from 35.67 to 642.41 m a.s.l. (Supplementary Fig. S5c). With the equilibrium line set at an altitude of 450 m a.s.l. (Noël et al. 2020), the mean elevation of 113 (79%) SCs lay below this isoline. The relief within SCs ranged from 258 to 1198 m, indicating a high degree of variability in the relative height of the area (Fig. 1, Supplementary Fig. S5g). Twenty-nine SCs had values of up to 500 m, while 112 had values between 500 and 1000 m. Only two SCs exceeded the 1000 m relative height difference, reaching 1185 and 1198 m, respectively. In 23 cases, the relief ratio was less than 0.1; in 93 cases, it was between 0.1 and 0.2; in 21 cases, it was between 0.2 and 0.3; and in six cases, it was above 0.3, with a maximum value of 0.37 (Supplementary Fig. S5h). This indicates a strong tendency for potential slope processes, especially as the permafrost that currently stabilizes the frozen ground progressively degrades.

The mean slope value ranged from 5.19° to 32.68° (Supplementary Fig. S4f). Even though it is likely that the mean slope of the terrain does not accurately represent the morphometry of a specific SC, the parameter is useful as it indicates the topographical variability in the research area. In 66 cases, the mean slopes were highly inclined (10–20°), and 63 were steep (20–35°); just 14 SCs were poorly inclined (0–5°). A predominantly southwest exposure was the most common, with 38 SCs exhibiting it. Fourteen SCs had a mostly southern exposure, and four faced mainly the south-east. Only 12 SCs were mainly exposed to the north (Supplementary Fig. S5e).

The circulatory ratios—where 0 is a line, and 1 is a circle (Shekar & Mathew 2024)—of the SCs ranged from 0.1 to 0.46 (Supplementary Fig. S5k). On the basis of morphometric analyses in the literature (Pareta & Pareta 2011; Shekar & Mathew 2024), 51 of the SCs in our study can be classified as elongated, 91 as more elongated, and one as circular (Supplementary Fig. S5j). The elongation ratios and form factors (Chandrashekar et al. 2015; Shekar & Mathew 2024) correspond well: 142 SCs classified as elongated had a form factor between 0.07 and 0.39, and one (Revdalen) that was more circular had a form factor of 0.89 (Supplementary Fig. S5i).

Changes in glacier extent. We assessed changes in glacial extent in the study area using satellite imagery, although not all glaciers could be discerned in all of the images. Most of the analysed glacier surface was below the equilibrium line altitude, which we set at 450 m a.s.l. (Fig. 3; Noël et al. 2020). Using the data from 1936/38 and 2020, we calculated the percentage change in area in glaciated SCs (Figs. 4, 5; see also Supplementary Table S1). The north-western and southern parts of the study area—that is, the parts nearer the sea—had lost the most glaciated area. SCs in the central part of the WJL—further inland and at higher elevations—lost the least amount of glaciated area, and there were even a few instances of positive glacial changes. The area of 16 glaciers has shrunk by more than 90% since 1936, and 43 glaciers have lost more than half of their area (Figs. 4, 5).

Comparing the 1936 and 2020 data revealed changes in glacier extent. The vast majority (94%) of the analysed glaciers have shrunk, with the following changes observed: 11 lost up to <10% of their area, 37 lost between 10 and 50%, 27 lost between 50 and 90% and 16 disappeared completely. In contrast, six glaciers increased in size by 1–15%. Overall, the area covered by glaciers shrank by just over 30%, from 228.34 km² in 1936 to 158.26 km² in 2020.

Lake evolution. We managed to discern only eight lakes within SCs on the 1936 orthophotomap (Supplementary Table S1, sheet lakes). This is because the orthophotomap was composed from oblique aerial images, and many places where we would expect lakes could not be spotted. An examination of the most detailed (0.4-m resolution) data source—the NPI orthophotomap of 2011—yielded 75 lakes within SCs (Supplementary Table S1). The number of lakes detected and the calculated areas (Supplementary Table S1) were affected by data quality issues, such as cloud cover and mountain shadows. In the Planet images, mountain shadows were problematic, and not all the lakes (or parts of lakes) could be identified even after enhancement, making it impossible to accurately calculate lake areas. Nonetheless, we see a general trend in the area of lakes expanding in the evolution of Svalbard's glacial lakes (Wieczorek et al. 2023), indicating their continuous growth (total area) with changes in the number of glacial lakes (merging of lakes). The available data are insufficient to provide a reliable analysis of the geomorphic influence on lakes.

Lakes located further away from glaciers seemed more stable, while those in contact with glaciers or moraines showed greater changes in area. In some cases—like that illustrated in Fig. 6a—there was a significant loss of surface area covered by the lake, whereas lake area increased in other cases—as shown in Fig. 6b. In both of these cases, lakes were located within moraines. As glaciers receded, some lakes emerged and, in most cases, were located at moraines (Fig. 6a–e). Those located in the lower parts of basins seemed more stable (Fig. 6f), as their forms were defined a long time ago.

Vegetation. For each SC, the difference between the oldest and youngest maximum NDVI values was calculated to assess how it changed over the last 40 years (Fig. 7).

Citation: *Polar Research* 2026, *45*, 12280, http://dx.doi.org/10.33265/polar.v45.12280

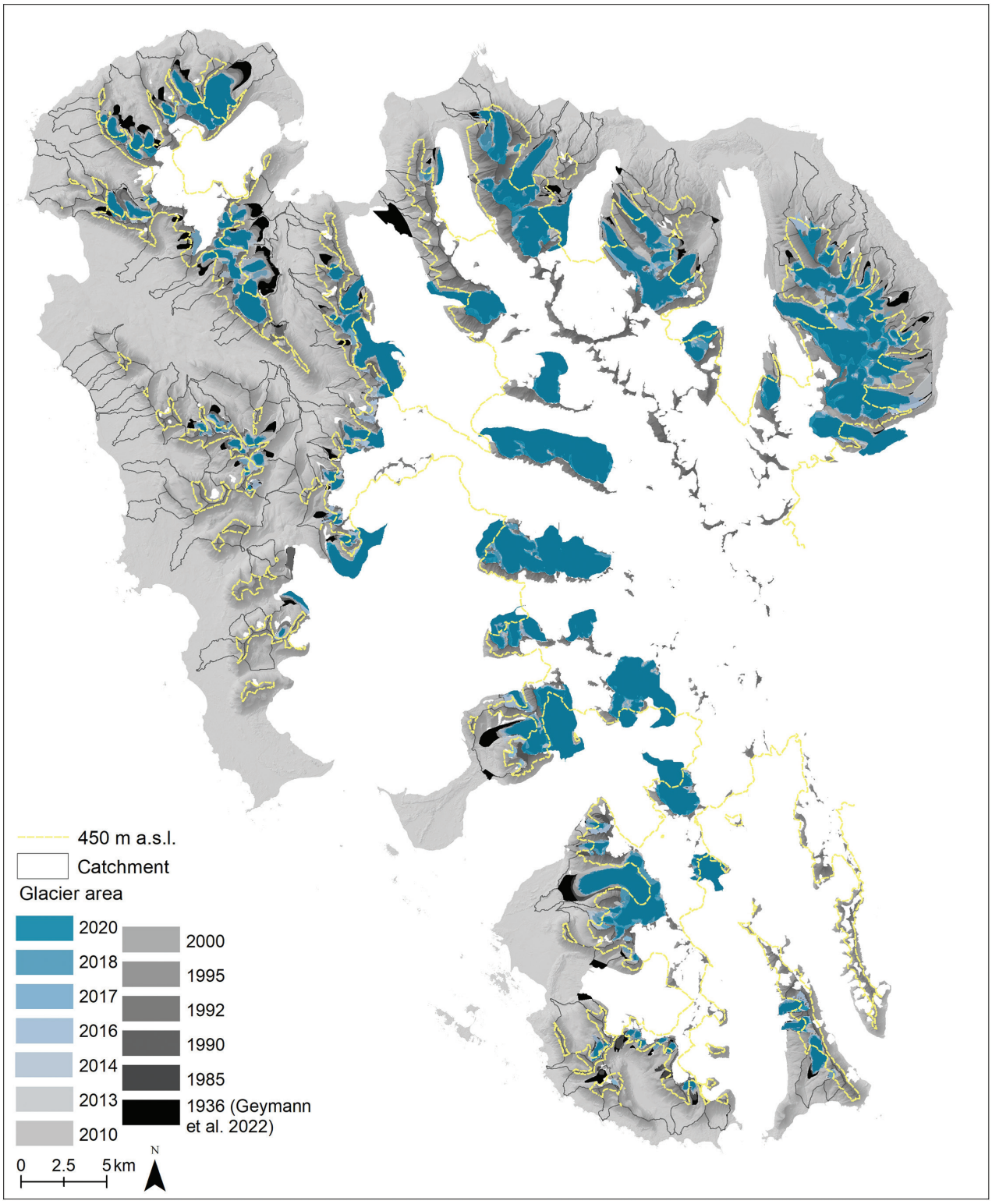

Fig. 3 Glacier areal change through time: 1936/38 (Geyman et al. 2022), 1985–2020 (USGS 2022), 1990 (NPI 2014b), 2017, 2018 and 2020 (Sentinel no date b). The contour at 450 m a.s.l. represents the equilibrium line altitude and is shown as a yellow dashed line (Noël et al. 2020).

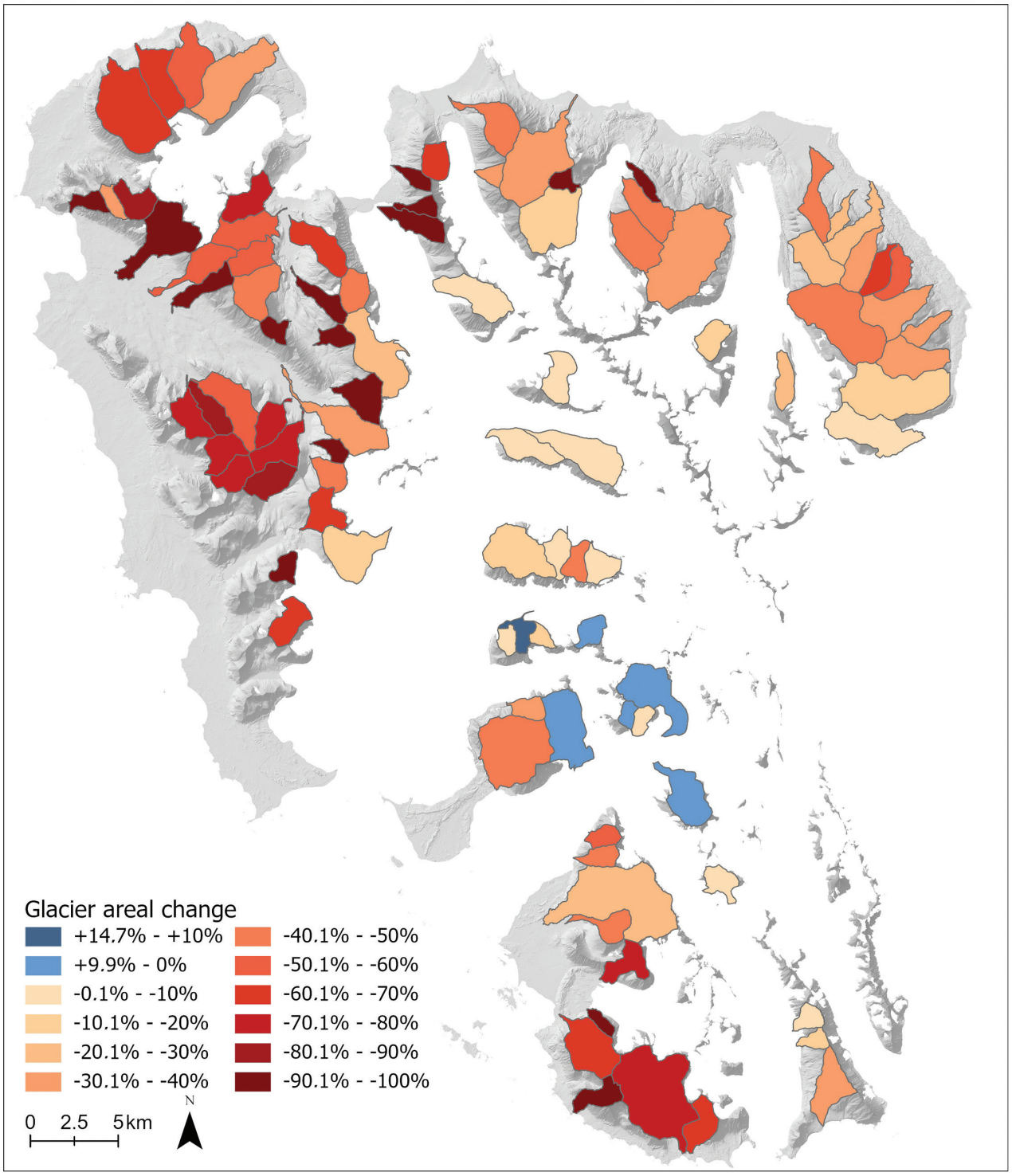

Fig. 4 Percentage changes in glacier area in glaciated SCs between 1936/38 (Geyman et al. 2022) and 2020.

In the vegetation analysis, there were 4592 observations for all the SCs (one observation is one SC in one satellite image) and, on the basis of these data, the maximum NDVI value for each SC for each year was calculated (Fig. 8). It is important to note that the number of SCs represented in the data varied as not all SCs were visible on each satellite image (see Supplementary Fig. S4) on account of different in paths, rows or cloud cover.

Citation: *Polar Research* 2026, *45*, 12280, http://dx.doi.org/10.33265/polar.v45.12280

The Mann–Kendall analysis of the NDVI data showed that only 21 of 143 SCs had a positive trend (Supplementary Table S1). Kendall's tau values for SCs with trends ranged from 0.3 to 0.4, where 0 is no monotonic trend, and 1 is a perfect positive trend. The remaining SCs showed no trend.

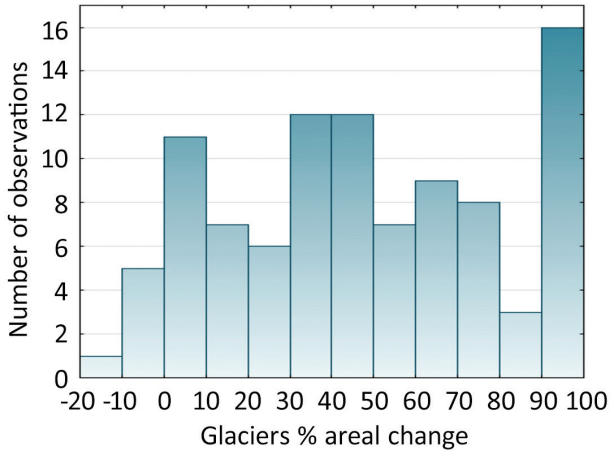

Fig. 5 Quantitative distribution of the percentage change in glacier area between 1939 (Geyman et al. 2022) and 2020.

The change in maximum NDVI in the southern SCs was notable, with the index reaching as high as 0.76–1 (Fig. 7). The spatial distribution of changes in the maximum NDVI was diverse, and no clear cause of the variability was evident.

Linkage between morphometry, glacial retreat, and vegetation growth. No clear relationship was evident when individual parameters were compared one by one (Supplementary Fig. S6). The multivariate analysis showed that, for NDVI changes, with the coefficient of determination coefficient $r^2 = 0.86$ (Fig. 9a), the mean slope and aspect majority had the highest impact on the models compared to other geomorphic parameters. For glaciers (Fig. 9b), mean elevation and mean slope were the two most important factors with $r^2 = 0.77$. The model was matched based on the data presented in Supplementary Table S1.

To analyse the exposure, we used the majority value for each SC and then tracked changes in vegetation and glacier recession. Neither the vegetation index nor the glacial areal changes showed a specific aspectual pattern within SCs (Fig. 10).

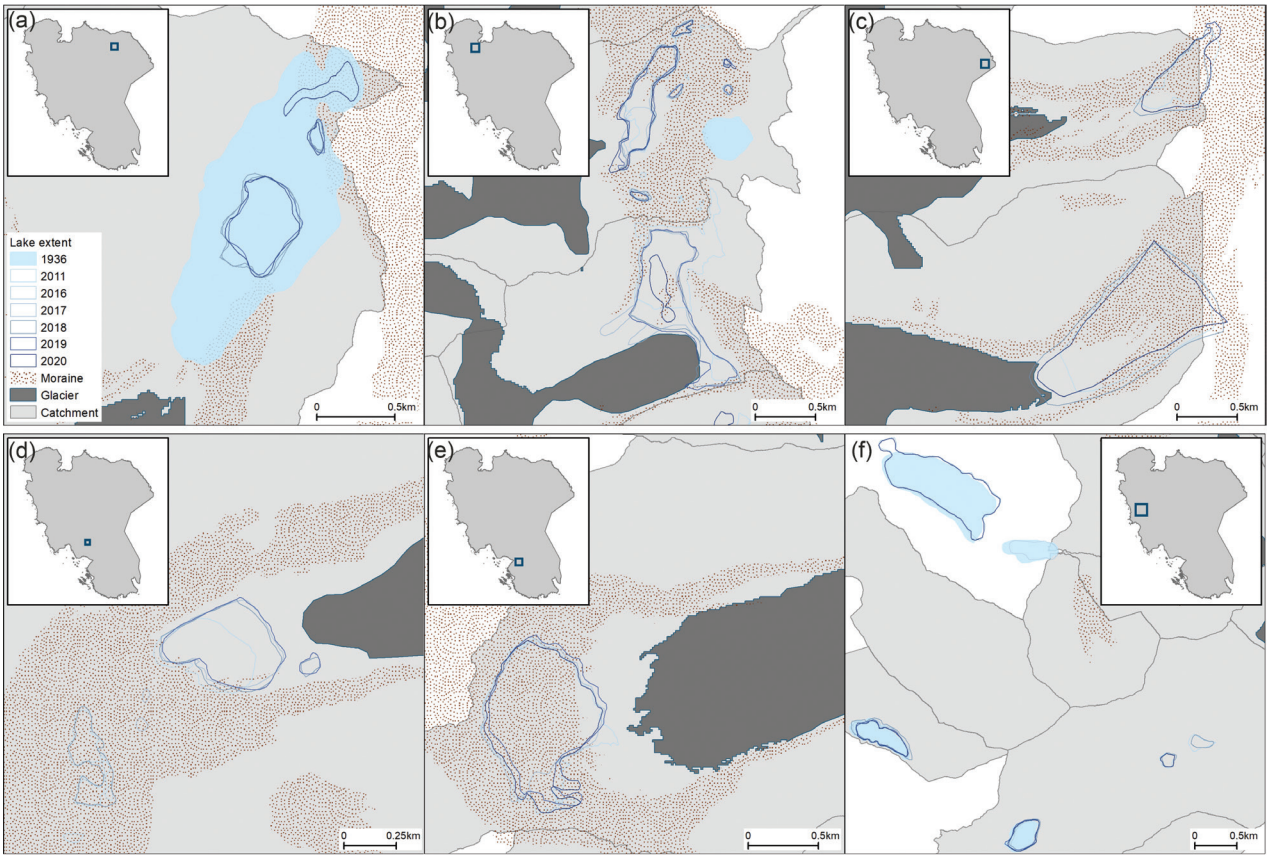

Fig. 6 Lake dynamics at selected sites in WJL.

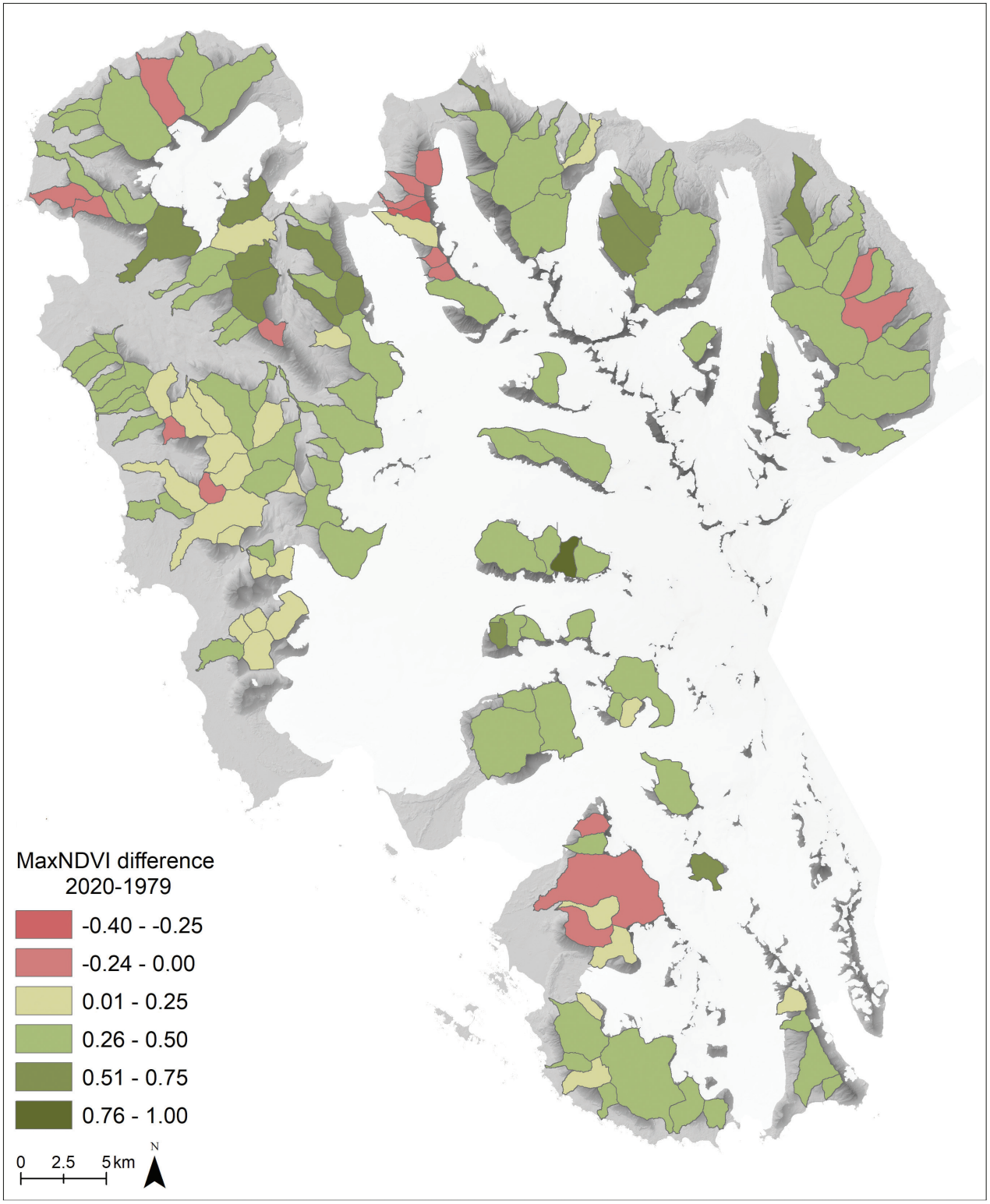

Fig. 7 The NDVI difference within SCs between the oldest (1979) and the newest (2020) measurements. Exact dates varied depending on image availability and cloud cover.

Citation: *Polar Research* 2026, *45*, 12280, http://dx.doi.org/10.33265/polar.v45.12280

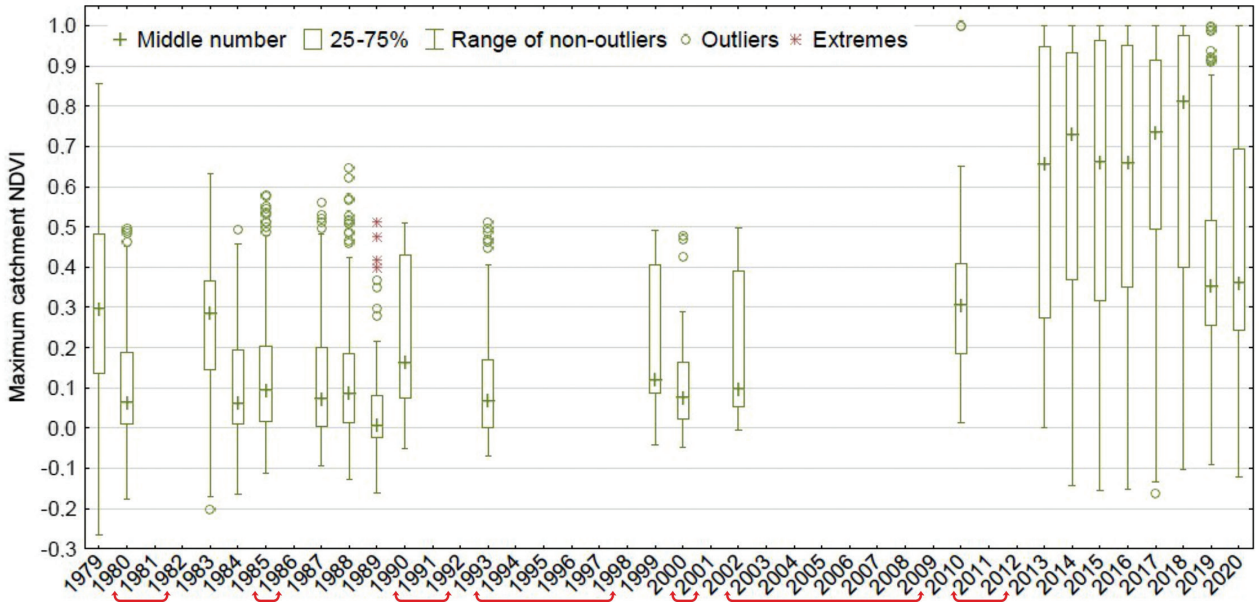

Fig. 8 Maximum NDVI values obtained for the SCs during the studied time. The underlined dates are those with no visible SCs in satellite imagery. Since 2013, the rise in maximum catchment NDVI is possibly linked to changes in the Landsat and Sentinel sensors.

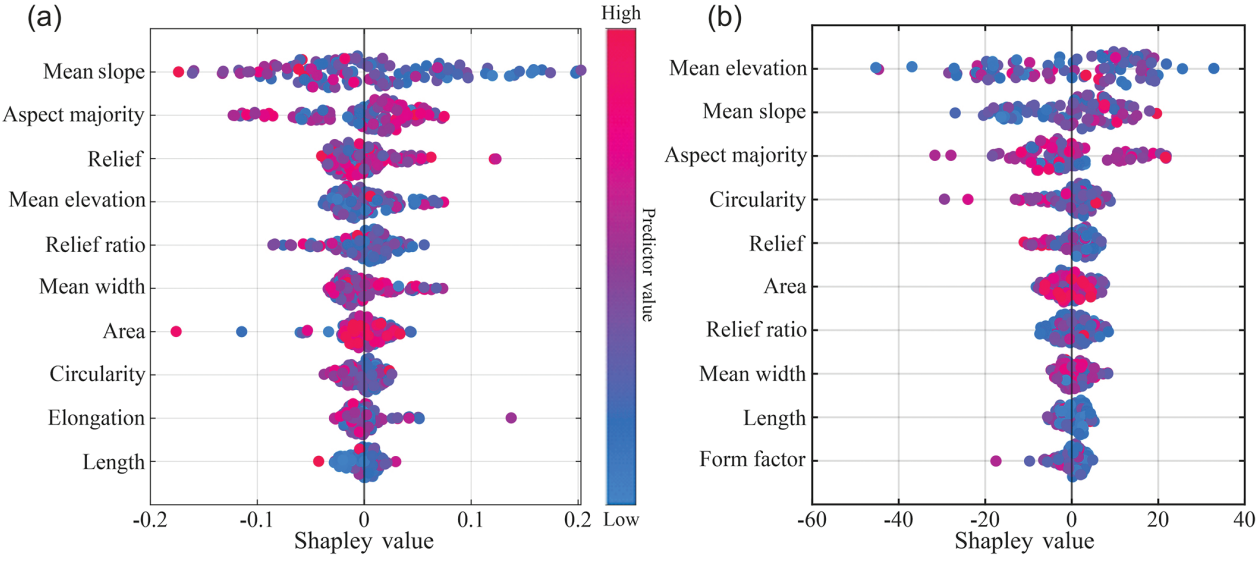

Fig. 9 Beeswarm plots showing the influence of individual morphometric features on (a) NDVI and (b) glaciers. The strength of the influence decreases from top to bottom.

Discussion

In delineating the SCs in the different elevation models, we encountered several problems. Firstly, the SCs differed across models due to varying model resolutions, which determined the level of detail in the watersheds. Additionally, the landscape has undergone significant change, namely glacial retreat, revealing numerous ice-cored moraines and uneven topography in the lower parts of SCs. As our research shows, there has been a clear and consistent glacial recession since 1936, which has resulted in the exposure of hills and ridges that were previously obscured by glacial ice. These features of the terrain can create multiple catchments where there was previously only one (e.g., Supplementary Fig. S7). Glacier lake outburst floods—another consequence of glacial

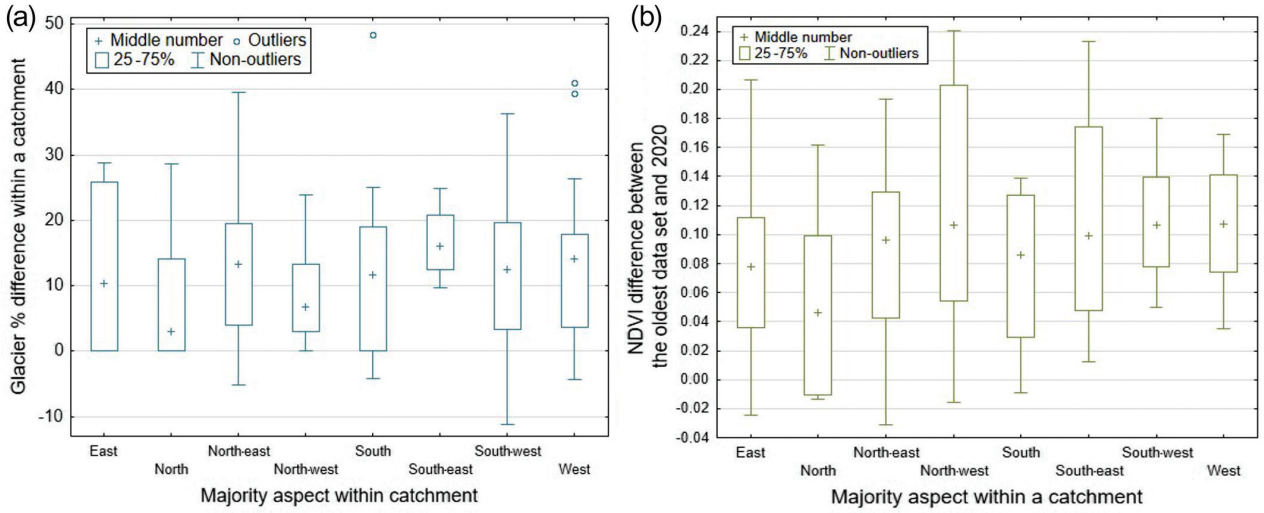

Fig. 10 Box and whisker plots for the majority (a) aspect and (b) changes in NDVI and glacier changes.

retreat—can shift the mouths of basins. These processes and events change SC areas. All climatic scenarios indicate that these changes will occur more frequently as a consequence of accelerated glacial retreat and the thickening of the active layer (Constable et al. 2022).

One of the biggest problems encountered in studies that use remotely sensed data is the frequent presence of clouds and shadows in Svalbard imagery (Meyers-Smith et al. 2020; Karlsen et al. 2024). Cirrus clouds are not always detected. We used the NDVI to minimize this effect on our vegetation analysis (Kääb 2005). Combined with the low angle of sunlight at this high latitude (>76°N), the mountainous terrain in our study area, including many sharp ridges and peaks casts shadows that can affect calculations. These can be manually addressed (e.g., using the darkest object subtraction method), but this practice becomes less feasible when a large number of catchments is analysed over a long time period (with different flight angles and paths producing different shadowing).

From 1936 to 2010, glaciers in southern Svalbard decreased in area by 800 km^2 (Geyman et al. 2022), and we observed a loss of 70 km^2 in the area of small glaciers analysed in this study. Svalbard's equilibrium line is located at ca. 450 m a.s.l. (Noël et al. 2020) and almost no SC glaciers in WJL are at this height; in some cases, only the topmost parts are at this height (Fig. 3). This will lead to further glacial recession in the area. An elevation study carried out on small (< 30 km^2) land-terminating mountain glaciers showed that elevation change in WJL varied from −1.4 to −1 m each year, which is among the highest values in Svalbard (Małecki 2022). Even though glacial retreat is slower with land-terminating glaciers (Kavan, Tallentire et al. 2022), a similar pace is predicted to result in the complete loss of ice cover in south-west Svalbard in the early 22nd century (Małecki 2022), where 16% of the total number of glaciers in the area have already vanished. The very last ice could be buried and preserved within moraine-like material (Luckman et al. 2015; Kavan, Tallentire et al. 2022). This provides us with an opportunity to observe the shift from glaciated to non-glaciated catchments and to track catchments' responses to reductions in ice.

The NDSI index was also intended to help us quantify the extent of snow cover within a given catchment area. However, the prevalence of high cloud cover made the data available for this purpose insufficient. It was often impossible to capture the melting of snow between full and residual snow cover within the catchments because no new data were collected at the time of transition. Consequently, this analysis was discontinued.

The change in annual total rainfall in Svalbard is +200 mm/year, and snowfall −60 mm/year, with rainfall comprising as much as 24% of total precipitation (Rawlins & Karmalkar 2024). The increase in rainfall will influence the intensity and size of mass movements (rock and soil), reinforced by the slope values (Supplementary Fig. S5f; Haeberli & Drenkhan 2022), as shown in a study of the McKenzie delta (Burn & Kokelj 2009). The ground stability is also linked to the active layer thickness. In the years 2000–2019, the active layer was ca. 0.9 m thick in southern Svalbard (Rawlins & Karmalkar 2024) or between 0.5 and 2 m (Nicu et al. 2024). Measurements in Bratteggdalen showed values from 1.5 up to 3.5/4 m (Kasprzak & Szymanowski 2023). Svalbard is predicted to have no permafrost by 2080–2099 (Rawlins & Karmalkar 2024). In WJL, 301 thaw slumps and 281 thermo-erosion gullies were detected, located mainly in the western and

Citation: *Polar Research* 2026, *45*, 12280, http://dx.doi.org/10.33265/polar.v45.12280

northern parts of WJL (Nicu et al. 2024). This trend may activate other geomorphic processes that may affect hydrography and vegetation.

The development of glacial lakes in Svalbard is directly linked to the end of the Little Ice Age (D'Andrea et al. 2012; Farnsworth et al. 2020; Wieczorek et al. 2023), as space forms between the moraine and the glacier front as the glacier melts. Many of the glacial lakes observed in the most recent time period of this study had not yet formed and were not observed in other studies dating to just a few years earlier (Rachlewicz et al. 2007; Małecki 2016; Geyman et al. 2022; Wieczorek et al. 2023). Post-glacial lakes are often formed on a moraine substrate that is mostly very arid and composed of unconsolidated material, with organic and chemical compounds derived mainly from glacial and slope meltwater (Modenutti et al. 2018). In non-glaciated valleys (such as Revvatnet in Revdalen), lakes are enriched with sediment and organic matter (Ruman et al. 2021). Vegetation thrives around them (e.g., Wołoszyn & Kasprzak 2023) compared to valleys where such water bodies are absent. The lakes also serve as sediment retention basins and play a crucial role in paraglacial processes (Kavan, Wieczorek et al. 2022; Dudek et al. 2023). During increased drainage of glacial lakes at the peak of the ablation season or extreme events such as glacial lake outburst floods, the runoff zone can be transformed (Dudek et al. 2023), new drainage areas can be created from proglacial zones (Wieczorek et al. 2024), and vegetation in the runoff zone can be covered by sediments or removed completely (Wołoszyn et al. 2022). This evolution in the proglacial landscape exemplifies dynamic changes in the High Arctic.

The vegetation response to anthropogenic climate change has been of scientific interest for over 30 years (Crawford et al. 1993). Changes in Arctic vegetation are heavily influenced by local conditions, with temperature as a primary driver of shrubification (García Criado et al. 2025). Our study revealed an increase in the NDVI index for only 22 catchments. More research is needed to make detailed conclusions about the impact of climate change on vegetation.

NDVI is widely used in polar regions and is useful for long time series, but it has limitations. First, images are not usable in a regular pattern, as the number of available images increases with the addition of new satellites. Moreover, the environment is captured in the exact atmospheric and hydrological conditions reflected in vegetation at a particular moment. NDVI is sensitive to highly diverse topography, which decreases the detection of sparse vegetation (Fretwell et al. 2011; Bayle et al. 2021) and of patchy vegetation on bare ground with surface water present on the surface (Berner et al. 2020). Multitemporal analyses are possible thanks to long Landsat time series of terrestrial ecosystems, but they are affected by sensor and data changes (Berner et al. 2023). The oldest Landsat images tend to yield lower NDVI values, which can result in a false positive trend over time (Berner et al. 2020; Berner et al. 2023). In one study, the NDVI obtained from the Landsat 8 OLI sensor was 0.0165 higher than that obtained from the Landsat 7 ETM+ sensor, corresponding to a mean difference of +4.86% relative to Landsat 7 ETM+ (Roy et al. 2016). Although the analysis of vegetation based solely on spectral responses that are proxies for photosynthesis cannot be considered as detailed research, it can indicate general trends in large-scale studies when fieldwork is difficult or impossible. In our study, NDVI values increased over time, but the vegetation advance was slow, perhaps limited by the paucity of nutrients in the ground. Higher index values, as observed in more recent, higher resolution images, can be effects of mosses and algae (Zmarz et al. 2023).

Conclusion

By 2100, a significant shift in our study area in southwest Svalbard is likely, as it changes from glaciated terrain to an environment that is more favourable for vegetation growth and mass movements of soil and rock. SCs will experience a marked decrease in glacial meltwater, an expansion of vegetation, and an interplay between vegetation advance and intensified mass movement. The number of lakes within SC is the most variable environmental feature and is expected to remain so during the transition from glaciated to non-glaciated conditions. This is especially true for lakes located near moraines and glaciers. Climatic factors exert the primary influence on the rate of deglaciation and vegetation development, but these are reinforced by topographic factors such as slope, aspect and elevation. Our research indicates that identifying areas most susceptible to climate change can be achieved by considering this combination of factors. SCs offer significant potential for detailed, holistic environmental analysis, facilitated by their small size, which allows for effective field research.

Acknowledgements

ArcticDEMs provided by the Polar Geospatial Center (University of Minnesota) under US National Science Foundation Office of Polar Programs awards 1043681, 1559691, 1542736, 1810976 and 2129685. The authors would like to thank Prof. S. Gruszczyński (AGH University of Krakow) for help with multivariate analysis. During the preparation of this work the authors used ChatGPT to write the initial version of the Python-2 scripts and to

check grammar and improve the writing. The authors reviewed and edited the content as needed and take full responsibility for it.

Funding

This study was supported by funding to the National Science Centre project CaLIA—Small Arctic Catchments in Post-Little Ice Age Conditions—Filling the Early 1960's Knowledge Gap for Small Catchments in the Wedel Jarlsberg Land (award no. 2023/49/N/ST10/01509) and to the National Science Centre project GLOWS (award no. 2023/49/N/ST10/01075). The research project was partly supported by the Excellence Initiative—Research University programme at the AGH University of Krakow. Further support came from a statutory research subsidy from the Department of Geomorphology at the Institute of Geography and Regional Development, University of Wrocław, Poland. IW was financially supported by the Polish National Agency for Academic Exchange Bekker programme (BPN/BEK/2025/1/00084).

Disclosure statement

The authors declare no conflict of interest.

References

Alphonse A.B., Wawrzyniak T., Osuch M. & Hanselmann N. 2023. Applying UAV-based remote sensing observation products in High Arctic catchments in SW Spitsbergen. *Remote Sensing 15*, article no. 934, doi: 10.3390/rs15040934.

Baye M. 2020. Watershed delineation by Arc Hydro tools. *International Journal of Science and Research 9*, 956–961, doi: 10.21275/SR20516144818.

Bayle A., Roussel E., Carlson B.Z., Vautier F., Brossard C., Fovet E., de Bouchard d'Aubeterre G. & Corenblit D. 2021. Sensitivity of Landsat NDVI to subpixel vegetation and topographic components in glacier forefields: assessment from high-resolution multispectral UAV imagery. *Journal of Applied Remote Sensing 15*, article no. 44508, doi: 10.1117/1.JRS.15.044508.

Berner L.T., Assmann J.J., Normand S. & Goetz S.J. 2023. "LandsatTS": an R package to facilitate retrieval, cleaning, cross-calibration, and phenological modeling of Landsat time series data. *Ecography 2023*, e06768, doi: 10.1111/ecog.06768.

Berner L.T., Massey R., Jantz P., Forbes B.C., Macias-Fauria M., Myers-Smith I., Kumpula T., Gauthier G., Andreu-Hayles L., Gaglioti B.V., Burns P., Zetterberg P., D'Arrigo R. & Goetz S.J. 2020. Summer warming explains widespread but not uniform greening in the Arctic tundra biome. *Nature Communications 11*, article no. 4621, doi: 10.1038/s41467-020-18479-5.

Box J.E., Colgan W.T., Christensen T.R., Schmidt N.M., Lund M., Parmentier F.-J.W., Brown R., Bhatt U.S., Euskirchen E.S., Romanovsky V.E., Walsh J.E., Overland J.E., Wang M., Corell R.W., Meier W.N., Wouters B., Mernild S., Mård J., Pawlak J. & Olsen M.S. 2019. Key indicators of Arctic climate change: 1971–2017. *Environmental Research Letters 14*, article no. 45010, doi: 10.1088/1748-9326/aafc1b.

Burn C.R. & Kokelj S.V. 2009. The environment and permafrost of the Mackenzie Delta area. *Permafrost and Periglacial Processes 20*, 83–105, doi: 10.1002/ppp.655.

Chandrashekar H., Lokesh K.V, Sameena M., Roopa J. & Ranganna G. 2015. GIS-based morphometric analysis of two reservoir catchments of Arkavati River, Ramanagaram District, Karnataka. *Aquatic Procedia 4*, 1345–1353, doi: 10.1016/j.aqpro.2015.02.175.

Constable A.J., Harper S., Dawson J., Holsman K., Mustonen T., Piepenburg D. & Rost B. 2022. Cross-chapter paper 6: polar regions. In H.-O. Pörtner et al. (eds.): *Climate change 2022: impacts, adaptation and vulnerability. Contribution of Working Group II to the sixth assessment report of the Intergovernmental Panel on Climate Change*. Pp. 2319–2368. Cambridge: Cambridge University Press.

Crawford R.M.M., Chapman H.M., Abbott R.J. & Balfour J. 1993. Potential impact of climatic warming on Arctic vegetation. *Flora 188*, 367–381, doi: 10.1016/S0367-2530(17)32286-7.

Dallmann W.K. (ed.) 2015. *Geoscience atlas of Svalbard*. *Report Series 148*. Tromsø: Norwegian Polar Institute.

D'Andrea W.J., Vaillencourt D.A., Balascio N.L., Werner A., Roof S.R., Retelle M. & Bradley R.S. 2012. Mild Little Ice Age and unprecedented recent warmth in an 1800 year lake sediment record from Svalbard. *Geology 40*, 1007–1010, doi: 10.1130/G33365.1.

Dømgaard M., Schomacker A., Isaksson E., Millan R., Huiban F., Dehecq A., Fleischer A., Moholdt G., Andersen J.K. & Bjørk A.A. 2024. Early aerial expedition photos reveal 85 years of glacier growth and stability in East Antarctica. *Nature Communications 15*, article no. 4466, doi: 10.1038/s41467-024-48886-x.

Dudek J., Wieczorek I., Suwiński M.K. & Strzelecki M.C. 2023. Paraglacial transformation and ice-dammed lake dynamics in a High Arctic glacier foreland, Gåsbreen, Svalbard. *Land Degradation and Development 34*, 4252–4271, doi: 10.1002/ldr.4773.

ESRI 2011. *Arc Hydro geoprocessing tools. Tutorial. Version 2.0.* New York, NY: ESRI. Accessed on the internet at https://content.esri.com/archydro/archydro/tutorial/doc/arc%20hydro%20gp%20tools%202.0%20-%20tutorial.pdf on 21 March 2024.

Farnsworth W.R., Allaart L., Ingólfsson Ó., Alexanderson H., Forwick M., Noormets R., Retelle M. & Schomacker A. 2020. Holocene glacial history of Svalbard: status, perspectives and challenges. *Earth-Science Reviews 208*, article no. 103249, doi: 10.1016/j.earscirev.2020.103249.

Florath J., Keller S., Abarca-del-Rio R., Hinz S., Staub G. & Weinmann M. 2022. Glacier monitoring based on multi-spectral and multi-temporal satellite data: a case study for classification with respect to different snow and

ice types. *Remote Sensing 14*, article no. 845, doi: 10.3390/rs14040845.

Førland E.J. & Hanssen-Bauer I. 2001. Changes in temperature and precipitation in the Norwegian Arctic during the 20th Century. In M.B. India & D.L. Bonillo (eds.): *Detecting and modelling regional climate change*. Pp. 153–161. Berlin: Springer.

Fretwell P.T., Convey P., Fleming A.H., Peat H.J. & Hughes K.A. 2011. Detecting and mapping vegetation distribution on the Antarctic Peninsula from remote sensing data. *Polar Biology 34*, 273–281, doi: 10.1007/s00300-010-0880-2.

Frost G.V., Bhatt U.S., Macander M.J., Berner L.T., Walker D.A., Raynolds M.K., Magnússon R.Í., Bartsch A., Bjerke J.W., Epstein H.E., Forbes B.C., Goetz S.J., Hoy E.E., Karlsen S.R., Kumpula T., Lantz T.C., Lara M.J., López-Blanco E., Montesano P.M., Neigh C.S.R., Nitze I., Orndahl K.M., Park T., Phoenix G.K., Rocha A.V., Rogers B.M., Schaepman-Strub G., Tømmervik H., Verdonen M., Veremeeva A., Virkkala A.-M. & Waigl C.F. 2025. The changing face of the Arctic: four decades of greening and implications for tundra ecosystems. *Frontiers in Environmental Science Volume 13*, article no. 1525574, doi: 10.3389/fenvs.2025.1525574.

García Criado M., Myers-Smith I.H., Bjorkman A.D., Elmendorf S.C., Normand S., Aastrup P., Aerts R., Alatalo J.M., Baeten L., Björk R.G., Björkman M.P., Boulanger-Lapointe N., Butler E.E., Cooper E.J., Cornelissen J.H.C., Daskalova G.N., Fadrique B., Forbes B.C., Henry G.H.R., Hollister R.D., Høye T.T., Jacobsen I.B.D., Jägerbrand A.K., Jónsdóttir I.S., Kaarlejärvi E., Khitun O., Klanderud K., Kolari T.H.M., Lang S.I., Lecomte N., Lenoir J., Macek P., Messier J., Michelsen A., Molau U., Muscarella R., Nielsen M.-L., Petit Bon M., Post E., Raundrup K., Rinnan R., Rixen C., Ryde I., Serra-Diaz J.M., Schaepman-Strub G., Schmidt N.M., Schrodt F., Sjögersten S., Steinbauer M.J., Stewart L., Strandberg B., Tolvanen A., Tweedie C.E. & Vellend M. 2025. Plant diversity dynamics over space and time in a warming Arctic. *Nature 642*, 653–661, doi: 10.1038/s41586-025-08946-8.

Geyman E.C., van Pelt J.J.W., Maloof A.C., Aas H.F. & Kohler J. 2022. Historical glacier change on Svalbard predicts doubling of mass loss by 2100. *Nature 601*, 374–379, doi: 10.1038/s41586-021-04314-4.

Haeberli W. & Drenkhan F. 2022. Future lake development in deglaciating mountain ranges. In L.S. Cutter (ed.): *Oxford research encyclopedia of natural hazard science*. Oxford: Oxford University Press. Doi: 10.1093/acrefore/9780199389407.013.361.

Hagolle O., Huc M., Desjardins C., Auer S. & Richter R. 2017. MAJA ATBD algorithm theoretical basis document. Doi: 10.5281/zenodo.1209633. Accessed on the internet at https://zenodo.org/records/1209633 on 2 March 2023.

Horton R.E. 1932. Drainage-basin characteristics. *Eos, Transactions American Geophysical Union 13*, 350–361, doi: 10.1029/TR013i001p00350.

Isaksen K., Nordli Ø., Ivanov B., Køltzow M.A.Ø., Aaboe S., Gjelten H.M., Mezghani A., Eastwood S., Førland E., Benestad R.E., Hanssen-Bauer I., Brækkan R., Sviashchennikov P., Demin V., Revina A. & Karandasheva T. 2022. Exceptional warming over the Barents area. *Scientific Reports 12*, article no. 9371, doi: 10.1038/s41598-022-13568-5.

Kääb A. 2005. *Remote sensing of mountain glaciers and permafrost creep*. *Schriftenreihe Physische Geographie Glaziologie und Geomorphodynamik 48*. Zurich: Universität Zürich.

Karlsen S.R., Elvebakk A., Stendardi L., Høgda K.A. & Macias-Fauria M. 2024. Greening of Svalbard. *Science of the Total Environment 945*, article no. 174130, doi: 10.1016/j.scitotenv.2024.174130.

Kasprzak M. & Szymanowski M. 2023. Spatial and temporal patterns of near-surface ground temperature in the Arctic mountain catchment. *Land Degradation and Development 34*, 5238–5258, doi: 10.1002/ldr.4841.

Kavan J., Tallentire G.D., Demidionov M., Dudek J. & Strzelecki M.C. 2022. Fifty years of tidewater glacier surface elevation and retreat dynamics along the south-east coast of Spitsbergen (Svalbard archipelago). *Remote Sensing 14*, article no. 354, doi: 10.3390/rs14020354.

Kavan J., Wieczorek I., Tallentire G.D., Demidionov M., Uher J. & Strzelecki M.C. 2022. Estimating suspended sediment fluxes from the largest glacial lake in Svalbard to fjord system using Sentinel-2 data: Trebrevatnet case study. *Water 14*, article no. 1840, doi: 10.3390/w14121840.

Keshri A.K., Shukla A. & Gupta R.P. 2009. ASTER ratio indices for supraglacial terrain mapping. *International Journal of Remote Sensing 30*, 519–524, doi: 10.1080/01431160802385459.

Lønne I. & Lyså A. 2005. Deglaciation dynamics following the Little Ice Age on Svalbard: implications for shaping of landscapes at high latitudes. *Geomorphology 72*, 300–319, doi: 10.1016/j.geomorph.2005.06.003.

Luckman A., Benn D.I., Cottier F., Bevan S., Nilsen F. & Inall M. 2015. Calving rates at tidewater glaciers vary strongly with ocean temperature. *Nature Communications 6*, article no. 8566, doi: 10.1038/ncomms9566.

Małecki J. 2016. Accelerating retreat and high-elevation thinning of glaciers in central Spitsbergen. *Cryosphere 10*, 1317–1329, doi: 10.5194/tc-10-1317-2016.

Małecki J. 2022. Recent contrasting behaviour of mountain glaciers across the European High Arctic revealed by ArcticDEM data. *Cryosphere 16*, 2067–2082, doi: 10.5194/tc-16-2067-2022.

MathWorks 2025. *Shapley values in Statistics and Machine Learning Toolbox™*. The MathWorks Inc. Accessed on the internet at https://www.mathworks.com/products/statistics.html on 21 July 2025.

McCerery R., Davies B.J., Lovell H., Calvo-Ryan R., Pearce D.A., Małecki J. & Woodward J. 2025. Landsystem models from remote and field based geomorphological mapping reveal diverse glacier dynamics on Svalbard. *Geomorphology 484*, article no. 109854, doi: 10.1016/j.geomorph.2025.109854.

McKay D.I.A., Staal A., Abrams J.F., Winkelmann R., Sakschewski B., Loriani S., Fetzer I., Cornell S.E., Rockström J. & Lenton T.M. 2022. Exceeding 1.5°C global warming could trigger multiple climate tipping points. *Science 377*, article no. 6611, doi: 10.1126/science.abn7950.

Meyers-Smith I.H., Kerby J.T., Phoenix G.K., Bjerke J.W., Epstein H.E., Assmann J.J., John C., Andreu-Hayles L., Angers-Blondin S., Beck P.S.A., Berner L.T., Bhatt U.S., Bjorkman A.D., Blok D., Bryn A., Christiansen C.T., Cornelissen J.H.C., Cunliffe A.M., Elmendorf S.C., Forbes B.C., Goetz S.J., Hollister R.D., de Jong R., Loranty M.M., Macias-Fauria M., Maseyk K., Normand S., Olofsson J., Parker T.C., Parmentier F.-J.W., Post E., Schaepman-Strub G., Stordal F., Sullivan P.F., Thomas H.J.D., Tømmervik H., Treharne R., Tweedie C.E., Walker D.A., Wilmking M. & Wipf S. 2020. Complexity revealed in the greening of the Arctic. *Nature Climate Change 10*, 106–117, doi: 10.1038/s41558-019-0688-1.

Modenutti B., Bastidas Navarro M., Martyniuk N. & Balseiro E. 2018. Melting of clean and debris-rich ice differentially affect nutrients, dissolved organic matter and bacteria respiration in the early ontogeny of the newly formed proglacial Ventisquero Negro Lake (Patagonia Argentina). *Freshwater Biology 63*, 1341–1351, doi: 10.1111/fwb.13161.

Nicu I.C., Rubensdotter L., Tanyaş H. & Lombardo L. 2024. Near pan-Svalbard permafrost cryospheric hazards inventory (SvalCryo). *Scientific Data 11*, article no. 894, doi: 10.1038/s41597-024-03754-7.

Noël B., Jakobs C.L., van Pelt W.J.J., Lhermitte S., Wouters B., Kohler J., Hagen J.O., Luks B., Reijmer C.H., van de Berg W.J. & van den Broeke M.R. 2020. Low elevation of Svalbard glaciers drives high mass loss variability. *Nature Communications 11*, article no. 4597, doi: 10.1038/s41467-020-18356-1.

NPI (Norwegian Polar Institute) 2014a. Kartdata Svalbard 1:100 000 (S100 Kartdata) / Map data. Data set. Doi: 10.21334/NPOLAR.2014.645336C7. Accessed on the internet at https://data.npolar.no/dataset/645336c7-adfe-4d5a-978d-9426fe788ee3 on 25 May 2021.

NPI (Norwegian Polar Institute) 2014b. Terrengmodell Svalbard (S0 Terrengmodell). Terrain model data set. Doi: 10.21334/NPOLAR.2014.DCE53A47. Accessed on the internet at https://data.npolar.no/dataset/dce53a47-c726-4845-85c3-a65b46fe2fea on 9 November 2022 and 24 January 2024.

Nuth C., Kohler J., König M., Von Deschwanden A., Hagen J.O., Kääb A., Moholdt G. & Pettersson R. 2013. Decadal changes from a multi-temporal glacier inventory of Svalbard. *Cryosphere 7*, 1603–1621, doi: 10.5194/tc-7-1603-2013.

Pareta K. & Pareta U. 2011. Quantitative morphometric analysis of a watershed of Yamuna Basin, India using ASTER (DEM) data and GIS. *International Journal of Geomatics and Geosciences 2*, 248–269.

Porter C., Howat I., Noh M.-J., Husby E., Khuvis S., Danish E., Tomko K., Gardiner J., Negrete A., Yadav B., Klassen J., Kelleher C., Cloutier M., Bakker J., Enos J., Arnold G., Bauer G., Morin P., Foundation N.S. & NASA. 2023. *ArcticDEM. Mosaics, version 4.1*. Data set. Harvard Dataverse. doi: 10.7910/DVN/3VDC4W. Accessed on the internet at https://data.pgc.umn.edu/elev/dem/setsm/ArcticDEM/mosaic/v4.1/ on 8 April 2024.

Rachlewicz G., Szczuciński W. & Ewertowski M. 2007. Post-"Little Ice Age" retreat rates of glaciers around Billefjorden in central Spitsbergen, Svalbard. *Polish Polar Research 28*, 159–186.

Rantanen M., Karpechko A.Y., Lipponen A., Nordling K., Hyvärinen O., Ruosteenoja K., Vihma T. & Laaksonen A. 2022. The Arctic has warmed nearly four times faster than the globe since 1979. *Communications Earth and Environment 3*, article no. 168, doi: 10.1038/s43247-022-00498-3.

Rawlins M.A. & Karmalkar A.V. 2024. Regime shifts in Arctic terrestrial hydrology manifested from impacts of climate warming. *The Cryosphere 18*, 1033–1052, doi: 10.5194/tc-18-1033-2024.

Roy D.P., Kovalskyy V., Zhang H.K., Vermote E.F., Yan L., Kumar S.S. & Egorov A. 2016. Characterization of Landsat-7 to Landsat-8 reflective wavelength and normalized difference vegetation index continuity. *Remote Sensing of Environment 185*, 57–70, doi: 10.1016/j.rse.2015.12.024.

Roy D.P., Wulder M.A., Loveland T.R., Woodcock C.E., Allen R.R., Anderson M.C., Helder D., Irons J.R., Johnson D.M., Kennedy R., Scambos T.A., Schaaf C.B., Schott J.R., Sheng Y., Vermote E.F., Belward A.S., Bindschadler R., Cohen W.B., Gao F., Hipple J.D., Hostert P., Huntington J., Justice C.O., Kilic A., Kovalskyy V., Lee Z.P., Lymburner L., Masek J.G., McCorkel J., Shuai Y., Trezza R., Vogelmann J., Wynne R.H. & Zhu Z. 2014. Landsat-8: science and product vision for terrestrial global change research. *Remote Sensing of Environment 145*, 154–172, doi: 10.1016/j.rse.2014.02.001.

Różycka M. & Migoń P. 2021. Morphometric properties of river basins as indicators of relative tectonic activity—problems of data handling and interpretation. *Geomorphology 389*, article no. 107807, doi: 10.1016/j.geomorph.2021.107807.

Ruman M., Kosek K., Koziol K., Ciepły M., Kozak-Dylewska K. & Polkowska Ż. 2021. A High-Arctic flow-through lake system hydrochemical changes: Revvatnet, southwestern Svalbard (years 2010–2018). *Chemosphere 275*, article no. 130046, doi: 10.1016/j.chemosphere.2021.130046.

Schumm S. 1956. Evolution of drainage systems and slopes in badlands at Perth Amboy, New Jersey. *Geological Society of America Bulletin 67*, 597–646, doi: 10.1130/0016-7606(1956)67[597:EODSAS]2.0.CO;2.

Sentinel Hub no date a. Custom scripts. Accessed on the internet at https://custom-scripts.sentinel-hub.com/ on 6 March 2026.

Sentinel Hub no date b. EO Browser. Sentinel-2 satellite images. Contains modified Copernicus Sentinel data 2017, 2018, 2020 processed by Sentinel Hub. Accessed on the internet at https://www.sentinel-hub.com/explore/eobrowser/ on 22 April 2024.

Shekar P.R. & Mathew A. 2024. Morphometric analysis of watersheds: a comprehensive review of data sources, quality, and geospatial techniques. *Watershed Ecology and the Environment 6*, 13–25, doi: 10.1016/j.wsee.2023.12.001.

Smith D.M., Screen J.A., Deser C., Cohen J., Fyfe J.C., García-Serrano J., Jung T., Kattsov V., Matei D., Msadek R., Peings Y., Sigmond M., Ukita J., Yoon J.-H. & Zhang X. 2019. The Polar Amplification Model Intercomparison Project (PAMIP) contribution to CMIP6: investigating the causes and consequences of polar amplification.

Geoscientific Model Development 12, 1139–1164, doi: 10.5194/gmd-12-1139-2019.

Speetjens N.J., Hugelius G., Gumbricht T., Lantuit H., Berghuijs W.R., Pika P.A., Poste A. & Vonk J.E. 2022. ARCADE: The Pan-Arctic Catchment Database. *Earth System Science Data 15*, 541–554, doi: 10.34894/U9HSPV.

Stachnik Ł., Migała K., Wąsik M., Marszałek H., Wołoszyn A., Kasprzak M., Łepkowska E., Pilguj N., Ignatiuk D., Zielonka A. & Bartosiewicz M. 2025. Resolving the climate-controlled hydrological regime in a model permafrost catchment for future management strategies. *Journal of Environmental Management 383*, article no. 125189, doi: 10.1016/j.jenvman.2025.125189.

Stachowska Z., van der Bilt W.G.M. & Strzelecki M.C. 2024. Coastal lake sediments from Arctic Svalbard suggest colder summers are stormier. *Nature Communications 15*, article no. 9688, doi: 10.1038/s41467-024-53875-1.

Tobo Y., Adachi K., Kawai K., Matsui H., Ohata S., Oshima N., Kondo Y., Hermansen O., Uchida M., Inoue J. & Koike M. 2024. Surface warming in Svalbard may have led to increases in highly active ice-nucleating particles. *Communications Earth and Environment 5*, article no. 516, doi: 10.1038/s43247-024-01677-0.

Trenberth K., Anthes R.A., Belward A., Brown O.B., Haberman T., Karl T.R., Running S., Ryan B., Tanner M. & Wielicki B. 2013. Challenges of a sustained climate observing system. In G. Asrar & J. Hurrell (eds.): *Climate science for serving society. Research, modeling and prediction priorities.* Pp. 13–50. Dordrecht: Springer.

Tucker C.J. 1979. Red and photographic infrared linear combinations for monitoring vegetation. *Remote Sensing of Environment 8*, 127–150, doi: 10.1016/0034-4257(79)90013-0.

USGS (U.S. Geological Survey) 2021. *Landsat Collection 2 Level-2 science products*. *U.S. Geological Survey Fact Sheet 2021–3055*. Doi: 10.3133/fs20213055. Accessed on the internet at https://pubs.usgs.gov/publication/fs20213055 on 15 October 2024.

USGS (U.S. Geologcial Survey) 2022. EarthExplorer. Data set. Accessed on the internet at https://earthexplorer.usgs.gov/ on 11 March 2024.

Vincent W.F. 2020. Arctic climate change: local impacts, global consequences, and policy implications. In C. Coates et al. (eds.): *The Palgrave handbook of Arctic policy and politics*. Pp. 507–526. Cham: Springer.

Vonk J.E., Speetjens N.J. & Poste A.E. 2023. Small watersheds may play a disproportionate role in Arctic land–ocean fluxes. *Nature Communications 14*, article no. 3442, doi: 10.1038/s41467-023-39209-7.

Wawrzyniak T. & Osuch M. 2020. A 40-year High Arctic climatological dataset of the Polish Polar Station Hornsund (SW Spitsbergen, Svalbard). *Earth System Science Data 12*, 805–815, doi: 10.5194/essd-12-805-2020.

Wieczorek I., Kavan J., Wołoszyn A., Yde J., Stachnik Ł., Zagórski P. & Strzelecki C. 2024. Development of a glacial lake system during High Arctic paraglacial landscape transformation at Crammerbreane glacier system, Svalbard. Unpublished ms. Accessed on the internet at https://ssrn.com/abstract=4720879 on 24 November 2024.

Wieczorek I., Strzelecki M.C., Stachnik Ł., Yde J.C. & Małecki J. 2023. Post-Little Ice Age glacial lake evolution in Svalbard: inventory of lake changes and lake types. *Journal of Glaciology 69*, 1449–1465, doi: 10.1017/jog.2023.34.

Wołoszyn A. 2024. Featured data sources and normalised indices of use in small Arctic catchment research. *Quaestiones Geographicae 43*, 257–266, doi: 10.14746/quageo-2024-0015.

Wołoszyn A. & Kasprzak M. 2023. Contemporary landscape transformation in a small Arctic catchment (Bratteggdalen, Svalbard). *Polish Polar Research 44*, 227–248, doi: 10.24425/ppr.2023.144542.

Wołoszyn A., Owczarek Z., Wieczorek I., Kasprzak M. & Strzelecki M.C. 2022. Glacial outburst floods responsible for major environmental shift in Arctic coastal catchment, Rekvedbukta, Albert I Land, Svalbard. *Remote Sensing 14,* article no. 6325, doi: 10.3390/rs14246325.

Wulder M.A., Roy D.P., Radeloff V.C., Loveland T.R., Anderson M.C., Johnson D.M., Healey S., Zhu Z., Scambos T.A., Pahlevan N., Hansen M., Gorelick N., Crawford C.J., Masek J.G., Hermosilla T., White J.C., Belward A.S., Schaaf C., Woodcock C.E., Huntington J.L., Lymburner L., Hostert P., Gao F., Lyapustin A., Pekel J.F., Strobl P. & Cook B.D. 2022. Fifty years of Landsat science and impacts. *Remote Sensing of Environment 280*, article no. 113195, doi: 10.1016/j.rse.2022.113195.

Yamanouchi T. & Takata K. 2020. Rapid change of the Arctic climate system and its global influences—overview of GRENE Arctic climate change research project (2011–2016). *Polar Science 25*, article no. 100548, doi: 10.1016/j.polar.2020.100548.

Zmarz A., Karlsen S.R., Kycko M., Korczak-Abshire M., Gołębiowska I., Karsznia I. & Chwedorzewska K. 2023. BVLOS UAV missions for vegetation mapping in maritime Antarctic. *Frontiers in Environmental Science 11*, article no. 1154115, doi: 10.3389/fenvs.2023.1154115.